

# Effect of density on the hygroscopicity and surface characteristics of hybrid poplar compreg

Minzhen Bao<sup>1</sup> · Xianai Huang<sup>2</sup> · Yahui Zhang<sup>1</sup> · Wenji Yu<sup>1</sup> · Yanglun Yu<sup>1</sup>

Received: 8 May 2016 / Accepted: 24 June 2016 / Published online: 6 July 2016  
© The Japan Wood Research Society 2016

**Abstract** The objective of this study is to investigate the relevance of hybrid poplar compreg density and its physical properties and surface characteristics, such as hygroscopicity, dimensional stability, wettability, roughness, surface energy, and porosity. The different desired densities (ranging from 0.6 to 1.2 g/cm<sup>3</sup>) of compreg were achieved using manufacturing processes with various parameters. The results indicated that the water absorption decreased and dimensional stability improved with the density increasing in the range of this study. In addition, the density was contributed to the reduction of the wettability and the roughness of compreg. Furthermore, the evaluation of the surface energy showed that the total surface free energy declined significantly due to the densification process. The high density reduced the apertures present in the vessels and the fiber cells and, consequently, decreased the total porosity of compreg. This, in turn, impeded the penetration of moisture into compreg and reduced its hygroscopicity.

**Keywords** Compreg · Density · Hygroscopicity · Surface characteristics · Microstructure

## Introduction

China has long been committed to the cultivation of rapid growth forest, and the existing forest area has ranked the first in the world. Poplar is one of the widely planted fast-growing tree species in China, and its plantation area and stocking volume have reached 9.97 million hm<sup>2</sup> and 624 million m<sup>3</sup> according to the State Forestry Administration of China [1], respectively. Poplar is generally used in producing wood-based composites, such as plywood [2], particleboard [3], fiberboard [4], compressed wood [5], and fiber-reinforced polymer composites [6]. The output for poplar products increased to 4,700,000 m<sup>3</sup> in China, and there are several compressed poplar wood production factories with an ability of producing 150,000 m<sup>3</sup> plates yearly. However, the utilization of poplar wood is restricted due to its low-density and dimensional instability. Many studies have been performed aimed at enhancing performances of poplar by densification to increase the density and the mechanical strengths of the final wood product [7, 8].

Densification makes it possible for low-density woods to substitute for harder high-density species, so that the low-density wood species can be modified into high-performance and high-value products and gain commercial interest [9]. Several low-density wood species, such as spruce [10], radiata pine [11], oil palm [12], and poplar [13], have been extensively studied to be used as raw materials for producing compressed wood with a suitable manufacturing process, and the industrialization potentials of compressed wood made from these species are promising. However, the dimensional stability of the compressed poplar wood is still a challenging task, which limits its industrial application, specifically as an outdoor material. Compreg is a resin-treated compressed wood which is produced by treating solid wood or veneer with water-soluble phenol

✉ Wenji Yu  
chinayuwj@126.com

✉ Yanglun Yu  
yulunzi@163.com

<sup>1</sup> Key Laboratory of Wood Science and Technology of State Forestry Administration, Research Institute of Wood Industry, Chinese Academy of Forestry, Xiang Shan Road, Hai Dian District, Beijing 10091, People's Republic of China

<sup>2</sup> Université du Québec à Chicoutimi, Canada 555, Boul. de l'Université, Chicoutimi Québec G7H 2B1, Canada

formaldehyde resin and compressing to the desired density and thickness [14]. The phenol formaldehyde (PF) resin impregnation at considerably high pressure is one of the cost-effective ways to improve the dimensional stability of poplar compregs and enhance resistance to biological attack by reducing hygroscopicity [15, 16].

Nevertheless, poplar compregs are prone to deformation and cracking when they were used in a humid environment, especially in an outdoor environment [17]. High-density compreg shows better dimensional stability and physical and mechanical properties [18]. Therefore, there is need to study the complete theoretical research on the dimensional stability of poplar compreg density. Besides, high-density compreg manufacturing process can affect other properties [19, 20], such as wettability, roughness, microstructure, and porosity. There have been few report referred to the effect of density on the hygroscopicity and the surface characteristics of compressed wood. It is necessary to study and understand the mechanism of dimensional stability changes due to variation of compressed wood density.

The objective of this study was to produce compressed wood (compreg) using fast-growing poplar impregnated by low molecular weight phenol formaldehyde to investigate the influence of density on the hygroscopicity and surface characteristics of compregs. Besides, an attempt was carried out to build correlation between the changes of density with those of water resistance, surface wettability, and microstructure of compreg due to compressing process.

## Materials and methods

### Materials

Kiln-dried and rotary-peeled hybrid poplar veneers with the size of  $2.0 \pm 0.2 \text{ mm} \times 0.71 \times 1.27 \text{ m}$  were obtained from a mill located in the Shandong province of China. The samples were dried to the final moisture content of  $4.5 \pm 0.1 \%$ . The veneers, without insect holes and decay as well as with smooth surface, were visually selected, since the presence of defects may affect the appearance of the final products. Veneer sheets were cut into the nominal sizes of  $300 \times 85 \times 2 \text{ mm}$  (length  $\times$  width  $\times$  thickness) before manufacturing compreg. The PF resin used as the adhesive was acquired from Beijing Taier Chemical Co., Ltd. The PF had a solid content of 46.76 %, viscosity of 41 mPa s at 25 °C, and pH of 10–11.

### Compreg manufacturing

Air-dried wood veneers (4.5 % moisture content) were impregnated with 10 % PF resin in a vacuum pressure

impregnation tank to achieve 15 % resin content. The PF resin used in this study was diluted from the original PF.

Then, the resin-impregnated veneers were air dried to a moisture content of 10 %. The different desired densities (0.6, 0.7, 0.8, 0.9, 1.0, 1.1, and  $1.2 \text{ g/cm}^3$ ) were designed by controlling the weight of the dried veneers and the same final dimension of the compreg ( $300 \times 85 \times 6 \text{ mm}$ ). After weighing, the veneers were stacked and compressed together and heated for resin thermosetting at 140 °C for a time of 1 min/mm. Finally, the samples were unloaded at temperature of 30–40 °C. The experiments were replicated thrice for each condition. Thus, 21 reconstructed boards were manufactured. To reduce the density variations for the same sample, an edge of 15 mm for each panel was trimmed off.

### Characterization of physical properties

Rectangular strips of compreg samples with a dimension of  $20 \times 20 \times 6 \text{ mm}$  were cut and conditioned at the temperature of  $20 \pm 2 \text{ }^\circ\text{C}$  and the relative humidity (RH) of  $65 \pm 2 \%$  prior to the physical property testing. The specimens were immersed in water at 20 and 63 °C for 24 h according to the GB/T 17657-2013 [21] and GB/T 30364-2013 standard [22], respectively. After 24 h, the specimens were taken out and suspended to drain for 5 min to remove excess water. The mass and dimension of each specimen before and after immersing into water were determined and recorded at marked positions. The water absorption rate (WAR), width swelling rate (WSR), and thickness swelling rate (TSR) were calculated accordingly. Nine repetitions were carried out for each designed group, and the average results were obtained.

### Measurement of surface wettability

The wetting parameters obtained from the three test liquids (water, formamide, and diiodomethane) were significantly linked to the coating adhesion [23–25]. Therefore, the three liquids were chosen to determine the wettability behavior of compreg with different densities. The compreg samples were cut into small blocks with a size of  $40 \times 40 \times 6 \text{ mm}$ , and then, their tangential surfaces were sanded with 240-grit sand paper. The wetting behavior was determined on the tangential section of the samples by the sessile drop method with a JC2000D contact angle measuring instrument (Shanghai, China). Five tests were performed on each specimen, and two replicates were carried out for each group. An automatic micro syringe was used to dispense drops of approximately 4  $\mu\text{L}$  test liquid. The contact angle of droplet on each sample was measured at intervals of 1 s for the initial 10 and 2 s for the next 10 s after the liquid droplet fell down on the sample surface. As a reference, the contact angles on untreated wood sample surfaces were measured.

### Calculation of surface free energy

Direct measurement of surface free energy of solids is not feasible, which necessitates the indirect evaluation. The geometric mean model [26, 27] and Lifshitz-van der Waals/acid–base (LW–AB) [28] approach were applied in this study to calculate the surface free energy.

The geometric mean approach proposed by Wu [29] reported that the intermolecular energy between two materials resulted from the summation of a dispersion component ( $\gamma^d$ ) and a polar component ( $\gamma^p$ ). Since the surface free energy ( $\gamma$ ) is proportional to the intermolecular energy,  $\gamma$  itself can be considered as a sum of  $\gamma^d$  and  $\gamma^p$ . The interfacial energy ( $\gamma_L$ ) between a liquid polymer and a solid polymer can be evaluated by the geometric mean equation:

$$\gamma_L(1 + \cos\theta) = 2 \left( \sqrt{\gamma_S^d \gamma_L^d} + \sqrt{\gamma_S^p \gamma_L^p} \right) \tag{1}$$

where  $\theta$  is the contact angle, and the subscripts *S* and *L* denote solid and liquid phases, respectively.

The surface free energy of samples with various densities was also calculated by the LW–AB approach. According to this approach, the surface free energy is a sum of Lifshitz-van der Waals component ( $\gamma^{LW}$ ) and the acid–base ( $\gamma^{AB}$ ) component. The mathematical approach for the solid/liquid interfacial tension is given by

$$\gamma_L(1 + \cos\theta) = 2 \left( \sqrt{\gamma_S^{LW} \gamma_L^{LW}} + \sqrt{\gamma_S^+ \gamma_L^-} + \sqrt{\gamma_S^- \gamma_L^+} \right) \tag{2}$$

where  $\gamma^+$  denotes electron-accepting component, and  $\gamma^-$  is electron-donating component.

If the contact angles of at least three test liquids (with known surface free-energy components, see Table 1) are measured on the same solid surface, the surface free-energy components of the solid surface can be calculated using Eqs. (1) and (2). As a reference, the surface free-energy components of untreated wood samples were also summarized.

### Determination of surface roughness

The surface roughness of compreg samples was measured with a TIME 3230 surface roughometer. Specimens of 40 × 40 mm squares were cut and then sanded with 240-grit sand paper for 1 min. A Gaussian filter with a cut-off wavelength of 0.8 mm was used to transform the data.

Although several roughness parameters had been determined, the arithmetic average of the absolute deviations from the mean surface level (*Ra*) was used as the indicator of surface roughness. Three specimens were sampled for each group with the same density, and four random measurements of surface roughness were taken per specimen. As a reference, the surface roughness of untreated wood sample was measured.

### Evaluation of microstructure

The blocks with a size of 15 × 10 × 6 mm on the radial, tangential, and transverse sections were cut from untreated wood and compreg samples with four different densities (0.60, 0.80, 1.00, and 1.20 g/cm<sup>3</sup>). The samples were randomly selected from the specimens tested for surface wettability. Sections of 40 μm were sliced off from the three sections of each block using an ultramicrotome and then stained with a 1 % aqueous solution of safranin and stuck onto slides. They were dehydrated by means of a series of graded ethanol and embedded in Spurr resin for observation under a light microscope (Axio Imager A1, Germany).

### Evaluation of scanning electron microscope (SEM)

The bonding morphological features of the compreg samples were carried out by examining the micrographs produced by SEM. The specimens of 5 mm thick, which were cut from tangential section using microtome, were mounted on conductive adhesive tape. Then, the cutting surfaces were sputter-coated gold and scanned in an S4800 SEM with the magnification of up to 800,000×.

### Analysis of porosity

A Skyscan 1172 X-ray micro-tomography (μCT) with 0.5 μm micron pixel size supplied by Bruker Co., Ltd., Germany was used to analyze the porosity of compreg. The three specimens with the density of 0.6, 0.9, and 1.2 g/cm<sup>3</sup> were selected for the μCT analysis. To achieve the maximum resolution, the specimens (4 × 4 × 20 mm) were shaped to cylinders with a diameter of 2 mm, whereby the axis of these cylinders was chosen as the longitudinal direction of the samples. The specimens were stored under

**Table 1** Physical properties and surface free-energy components of test liquids

Liquid	Density (g/cm <sup>3</sup> )	Viscosity (mPa s)	Surface free energy (mJ/m <sup>2</sup> )						
			$\gamma_L$	$\gamma_L^d$	$\gamma_L^p$	$\gamma_L^{LW}$	$\gamma^{AB}$	$\gamma^+$	$\gamma^-$
Water	1.01	1.01	72.8	21.8	51.0	21.8	51.0	25.5	25.5
Formamide	1.13	2.93	58.0	39.0	19.0	39.0	19.0	2.28	39.6
Diiodomethane	3.33	3.35	50.8	50.8	0	50.8	0	0	0

the standard climate conditions (20 °C and 65 % relative humidity) until equilibrium moisture content was reached before the micro-tomography test. The specialized software, namely, CT analyser (CTAn), was used to analyze images and to calculate the total porosity, mean pore size (MPS), and to obtain the pore size distribution for each sample.

The theoretical porosity of wood was calculated according to the following equation:

$$C = 100 - (100\rho_{\text{od}}/\rho_{\text{cw}}) (\%) \quad (3)$$

where  $\rho_{\text{od}}$  is oven dry density and  $\rho_{\text{cw}}$  is the density of the wood cell wall, which is assumed as 1.53 g/cm<sup>3</sup> according to the literature [30]. The calculated theoretical porosity results were compared with those determined by CTAn.

### Statistical analysis

One-way analysis of variance (ANOVA) was conducted to study the effect of density on the surface properties of the composites at the 0.05 significance level. Duncan's multiple range test was employed to multiply compare the properties of composites with different densities. All the statistical analyses were performed using the software of IBM SPSS Statistics 22, with a significance level of 0.05 ( $p < 0.05$ ).

## Results and discussion

### Water resistance

It was well known that the water absorption of wood composites will result in the changes in dimensional, mechanical, and physical properties. Figure 1 demonstrates the effect of density on water absorption for composites in this study.

The WAR of composites reduced as the density of increased in both the cases of 20 and 63 °C. Higher density levels led to lower WAR of the composites. The WARs for composite with the density of 1.22 g/cm<sup>3</sup> were 4.5 and 2.9 times lower than those with the density of 0.60 g/cm<sup>3</sup> when immersed in water at temperature of 20 and at 63 °C, respectively.

The dimensional stability of the materials is especially important for the application evaluation of bio-based composites. Hence, the WSR and TSR of composite composites in water at two temperatures were determined. Figure 1b, c presented the curves of WSR and TSR as a function of density for composites when immersed in water at 20 °C and at 63 °C. The TSR and WSR of samples after immersion in water at the temperature of 63 °C were greater than those at 20 °C for all the same density. The tendencies of WSR due to density change showed similar

to those of WAR obtained in Fig. 1a. As the density increased, the WSR of the composites significantly decreased in both immersion temperatures (see Fig. 1b). The results indicate that the densification brings about an increase in dimensional stability.

It can be observed from Fig. 1c that the TSR of composites increased with density elevating from 0.60 to 0.90 g/cm<sup>3</sup>. Thereafter, there was a turn point appeared at the density of 0.90 g/cm<sup>3</sup>. The TSR started to reduce when the density continued to enhance from 0.90 to 1.22 g/cm<sup>3</sup> slightly for the case of 63 °C but obviously for the case of 20 °C. The results pointed out that the density of 0.90 g/cm<sup>3</sup> is the optimal density for composites in this study when refer to the thickness swelling. The similar trend has been reported for the TSR of bamboo composites with increased density [31].

From the analysis above, the water resistance of composites was attributed to the densification of the wood. The parenchyma tissues and vessels of wood were densified during the compression process. The PF resin penetrated into the cell lumen and a rigid cross-linking network was formed between resin and the cell wall during curing, which made the wood structure maintained in denser shape. Moreover, the swelling of the cell wall due to the penetration of resin into cell wall helps to increase dimensional stability [15, 32]. The mutually penetrated and interlocked structures of dense, thin-walled cells and phenol resin blocked the impregnation path of water [33]. Therefore, the hygroscopicity of composites was reduced.

### Surface wettability

The surface properties of densified wood can be changed because of the simultaneous effect of heat, moisture, and compression [19]. Increasing the density of the compressed wood alters the properties of bulk wood and the surface characteristics [34]. To study the influence of the density of the composite on the surface wettability, the polar liquids (distilled water and formamide) and non-polar liquid (diiodomethane) were used to investigate the change on the wettability during compressing process. The dynamic contact angles of the untreated wood and the composite of different densities were presented in Fig. 2.

Since wood is a porous material, the wetting process by liquids is usually accompanied by a process of fluid infiltration. Figure 2 presented the dynamic contact angles by three different liquids as a function of time for untreated wood and composites with different densities. As could be seen in the three figures, regardless test liquid types, the decreasing rate of contact angle with the time on the surface of the untreated wood was faster than those of composites. The higher is the density; the contact angles were

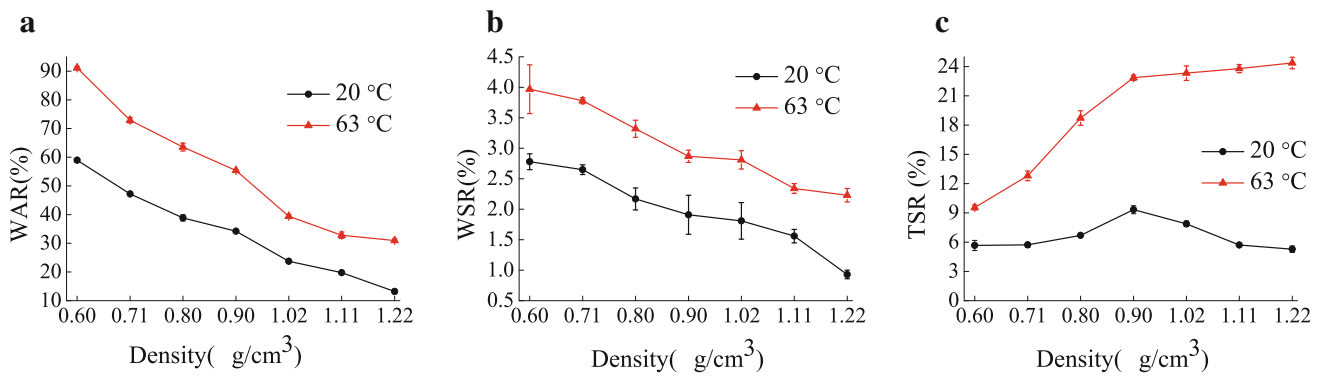


**Fig. 1** Water resistance of compregs as a function of density **a** water absorption rate (WAR); **b** width swelling rate (WSR); **c** thickness swelling rate (TSR)

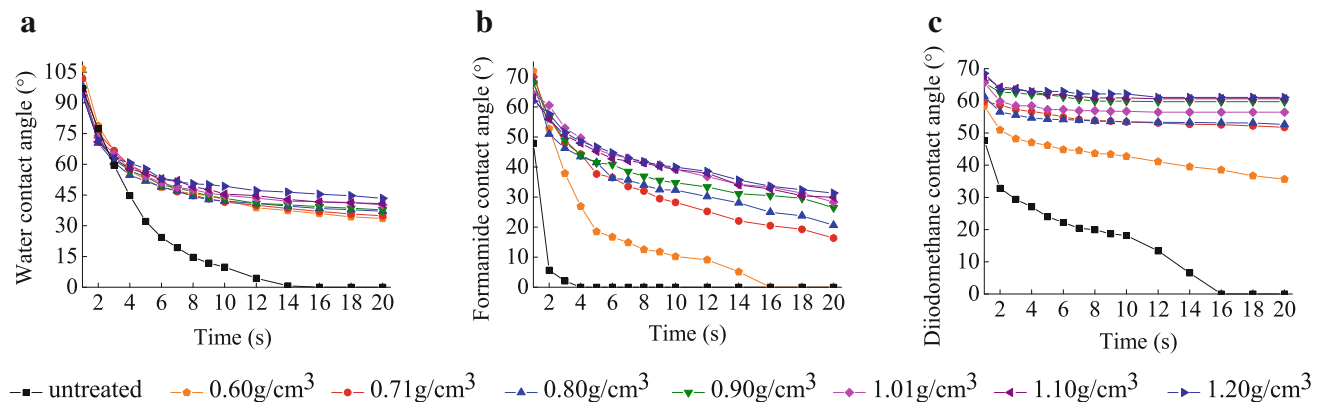


**Fig. 2** Effect of densities on dynamic contact angle of different liquids on untreated wood and compreg surfaces: **a** water, **b** formamide, and **c** diiodomethane

greater for all three liquids. The different wetting behaviors shown in Fig. 2 reflected the significant impact of the density on the wettability of compregs surface by both polar and non-polar liquids. As apparent in Fig. 2a, the contact angles at 20 s for compreg with density 1.20 g/cm³ increased to be 29.4 % higher than that of 0.60 g/cm³. Figure 2b showed that the greatest change in the contact angle of formamide with time was observed on untreated wood surface. The contact angle of untreated wood dropped substantially to zero within 4 s showing that the formamide was absorbed completely and quickly by the untreated wood. However, the decrease in the contact angle of compreg was relatively slow as the contacting time increased and there was still liquid left on the compregs surface even after 20 s. These indicated that compressing process decreased wettability of the compreg and this effect became more evident with higher density. As could be seen from Fig. 2c, there was a big difference in the contact angle of diiodomethane between the untreated wood and all the compregs. Within 4 s, all the samples showed decreases in the contact angles with increasing

time. After that, the untreated wood kept decreasing and dropped to zero at 16 s, while the compregs with densities more than 0.6 g/cm³ did not changed significantly and trended to reach equilibrium angles. The equilibrium contact angle of the compregs with the density of 1.20 g/cm³ was about 61.06°, which was over 25.38° larger than that of 0.60 g/cm³ at the same time. It can be concluded that the higher is density, the larger equilibrium contact angle on compreg surfaces. The increase in the contact angle of liquids on the compreg meant the lower wettability of the compreg, which was in agreement with the previous study [20].

The density of the compreg played a significant important role in its wettability. With the increase of the density, the wettability became worse. This could contribute to increase the water resistance of compreg. Moreover, the surface free energy is a critical property for the wetting and the coating on the compreg surface. Therefore, it is necessary to investigate the variation of the surface free energy of the untreated wood and the compregs with different densities.

## Surface free energy

The total surface free energy  $\gamma_S^T$  and its components were calculated for the untreated wood and the compreg specimens (see Table 2). Table 2 showed that, with the increase of the density,  $\gamma_S^d$  and  $\gamma_S^T$  decreased in the geometric mean model decreased, whereas  $\gamma_S^p$  showed the opposite trend. In addition,  $\gamma_S^d$  and  $\gamma_S^T$  were higher in the case of the untreated wood than that of the compreg.  $\gamma_S^d$  was higher than  $\gamma_S^p$  for all the samples, which was most likely due to the consequence of ageing surfaces [35, 36]. The previous studies [19, 37] of the surface free energy of hot-press wood had, however, reported a slight increase in  $\gamma_S^d$  after heat treatment. In this study, the decrease of  $\gamma_S^d$  and  $\gamma_S^T$  of the compreg surface may be attributed to the result of density.

In all the cases,  $\gamma_S^{LW}$  was the major surface free component compared to the acid–base components in acid–based model. Behavior of  $\gamma_S^{LW}$  changed after densification treatment.  $\gamma_S^+$  increased with the increasing density. As could be seen from the data in Table 2, regardless different models,  $\gamma_S^T$  were almost the same for the two models. The higher density considerably lowered  $\gamma_S^T$  of the compreg specimens. Taking into account the surface free-energy data of the compregs, it could be concluded that the densification and the PF resin during the compressing process lowered the surface energy and the non-polarity of wood.

## Surface roughness

Surface roughness is an important property in terms of surface quality, particularly in finishing processes. Rough surfaces of veneers reduce contact between them, resulting in a weak interaction with glue and low-strength properties of laminated veneer lumber (LVL) or plywood with the low-pressure processing [38]. Roughness at scale larger nanoscale will improve the wettability and penetration by veneer by adhesive. Moreover, with the high-pressure

compression process during manufacture compreg, the contact between the adjacent veneers is improved independent on the veneer surface condition. Hot pressing during compreg production mitigates the roughness of the final product by softening and compressing the compreg surface. The final sanding can improve the surface quality of compreg for finishing.

The values of surface roughness (*Ra*) with the standard deviations of the untreated wood and compregs with different densities were shown in Fig. 3. All densified compregs had lower *Ra* than that of untreated wood, and the roughness of compreg surface reduced with increasing density. The compreg with the density of 1.20 g/cm<sup>3</sup> had the smoothest surface with an *Ra* value of 1.02 μm, while the roughest surface was found for the control panel surface having an *Ra* value of 4.17 μm. The *Ra* of the compreg with the density of 1.20 g/cm<sup>3</sup> was 43.3 % lower than that of the compreg with density of 0.60 g/cm<sup>3</sup>. The density played an important role in decreasing the surface roughness. This means that the density increased during hot pressing improved the smoothness of compreg surface. Furthermore, the bulking of cell wall for both the fibers and the parenchyma due to the soaking into phenolic resin provided a more favorable surface for smooth. Both processes of pressing and bulking increase density and surface smoothness of compreg. Denser materials reduce the pore amount and the size of exited pore. Higher smoothness of surface means lower porosity of open pore exposed to moisture. These two effects of the entrance of moisture enter into wood substrate. These explained why all the compreg absorbed water slower that of untreated wood surface.

## Microstructure analysis

It was reported by Kutnar [39] that the densification of compreg was the result of the reduced lumen volume and buckling of the cell walls. Figure 4 presents the light

**Table 2** Surface tension components of untreated wood and compregs from geometric mean model and acid–base model

Density (g/cm <sup>3</sup> )	Surface free energy (mJ/m <sup>2</sup> )							
	Geometric mean model			Acid–base model				
	$\gamma_S^d$	$\gamma_S^p$	$\gamma_S^T$	$\gamma_S^{LW}$	$\gamma_S^+$	$\gamma_S^-$	$\gamma_S^{AB}$	$\gamma_S^T$
Untreated <sup>a</sup>	35.56	0.34	35.90	35.56	4.33	1.59	5.24	40.80
0.60	29.54	0.01	29.55	29.54	0.65	0.46	1.10	30.64
0.71	28.69	0.30	28.99	28.69	0.80	0.01	0.21	28.90
0.80	27.82	0.86	28.68	27.82	0.95	0.11	0.65	28.47
0.90	25.39	1.45	26.84	25.39	1.52	0.22	1.16	26.55
1.01	25.35	1.71	27.06	25.35	2.36	0.10	0.97	26.32
1.10	24.21	2.27	26.48	24.21	2.96	0.17	1.42	25.63
1.20	23.71	2.56	26.27	23.71	3.44	0.17	1.53	25.24

<sup>a</sup> The density of the untreated sample is 0.39 g/cm<sup>3</sup>

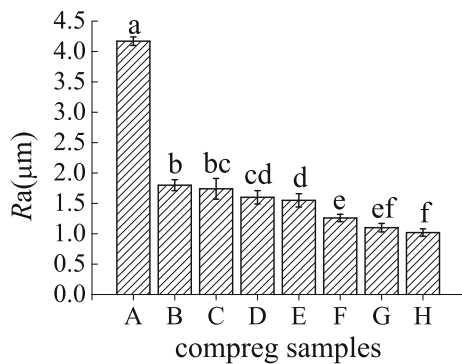


**Fig. 3** Roughness of untreated wood and compregs of different densities (A untreated hybrid poplar; B 0.60 g/cm<sup>3</sup>; C 0.71 g/cm<sup>3</sup>; D 0.80 g/cm<sup>3</sup>; E 0.90 g/cm<sup>3</sup>; F 1.01 g/cm<sup>3</sup>; G 1.10 g/cm<sup>3</sup>; H 1.20 g/cm<sup>3</sup>). The average values of roughness with different letters on the column indicated a significant difference at  $p < 0.05$  (analysis of variance (ANOVA), followed by Duncan's multiple range test)

microscope micrographs on three sections of untreated wood and compregs with three different densities.

As could be seen from Fig. 4a, hybrid poplar was a diffuse porous hardwood with slight difference between earlywood and latewood. The anatomic characteristics of the untreated hybrid poplar (homogeneous rays, thin-walled vessels and libriform fibers) were consistent with the results of the previous observations for poplars [40, 41]. The morphology of the compressed wood strongly depended upon the density (see Figs. 4b–e). Comparing with Fig. 4a, it could be seen that specimens of 0.60 g/cm<sup>3</sup> caused a deformation to the pores. The oval pores became irregular shapes, and the alignment had been tilted after compression. However, the pore size of the catheter did not change significantly (see Fig. 4b–3). The densities of 0.80 and 1.00 g/cm<sup>3</sup> were achieved a larger reduction in the void spaces of the wood (see Fig. 4c, d). The high strain in the manufacturing process drastically reduced the volume of void spaces in the specimens and deformed the cell lumens. The width of vessels in both radial and tangential sections was narrowed during the compressing process. When the density of compreg reached to 1.20 g/cm<sup>3</sup>, it had been very difficult to observe vessels in micrographs (see Fig. 4e1–3).

PF resins treatment improves dimensional stability for almost all wood-based products from composites to solid wood and densified solid wood [17, 18, 42]. Lower molecular weight PF resins are more easily to penetrate into the wood cell wall and ultimately bulk the wood material to a greater extent, thus providing greater stability [16]. PF resins appeared in vessels which were visible in Fig. 4. Higher density, indicative of higher stability, was maintained as resin concentrations increased. The image results confirmed that with the increase of compreg density, the amount of pores between cell wall decreased. This

thereby will improve the water resistance and reduce the surface wettability of compregs which shown in the results of Figs. 1 and 2.

### SEM analysis

Wood is a porous material, and there are a large number of holes and cell chambers on the surface and inner of wood, which are favorable conditions for the wood adhesive to enter and form adhesive force with wood cell wall. Figure 5 shows SEM images on the longitudinal tangential surface of untreated wood and compreg with the density of 1.20 g/cm<sup>3</sup>.

As apparent from Fig. 5, most of the pores inside the vessel and fiber narrowed and disappeared in the 1.20 g/cm<sup>3</sup> compreg exerting an influence on the liquid entrance into wood. Therefore, more mechanical bonding between adhesive and wood cells appeared in compreg, and it showed better water resistance. In addition, the cured PF resins filled in the gaps between vessels, fibers, and the wood rays can be observed in the SEM image of compreg sample (see Fig. 5b).

Mechanical adhesion theory [43] indicated that the gaps or holes on the surface of objects were filled with liquid adhesive and meshing connection occurred at the interface after the adhesive cured. This is the fundamental basis to understand the bonding between adhesive and wood for wood-based composites. For a more porous woody material, such as poplar, a portion of adhesive can over-penetrate the woody surface and others stay on the veneer surface for bonding purpose. Hence, the adhesive materials can penetrate into the cells which upon curing form an anchor (see Fig. 5b), at the same time leaving some parts of the adhesives on the veneer surface for adhesive transfer and bond formation with the adjacent veneer surface.

Here, two effects are brought about by adhesive. First, the adhesive covered on the surface of wood cells protects the cells against absorbing moisture. This improves the water resistance of compreg. Second, the bonding effect between the same or different wood cells, such as fibers, vessels, and wood rays leads to the connection of the organizations. The interacted force offered by the adhesive restricts the rebounding of dimension due to absorbance of moisture.

### Porosity analysis

The vessel lumen volume decreased due to compression progress which resulted in increasing density of compressed wood. Since the sizes of wood cells range in size from 1 to 100 μm, the X-ray micro-tomography scanning (μCT) with resolutions of few microns (0.5 μm) is suitable for the examination of wood cell in micro-scale. The

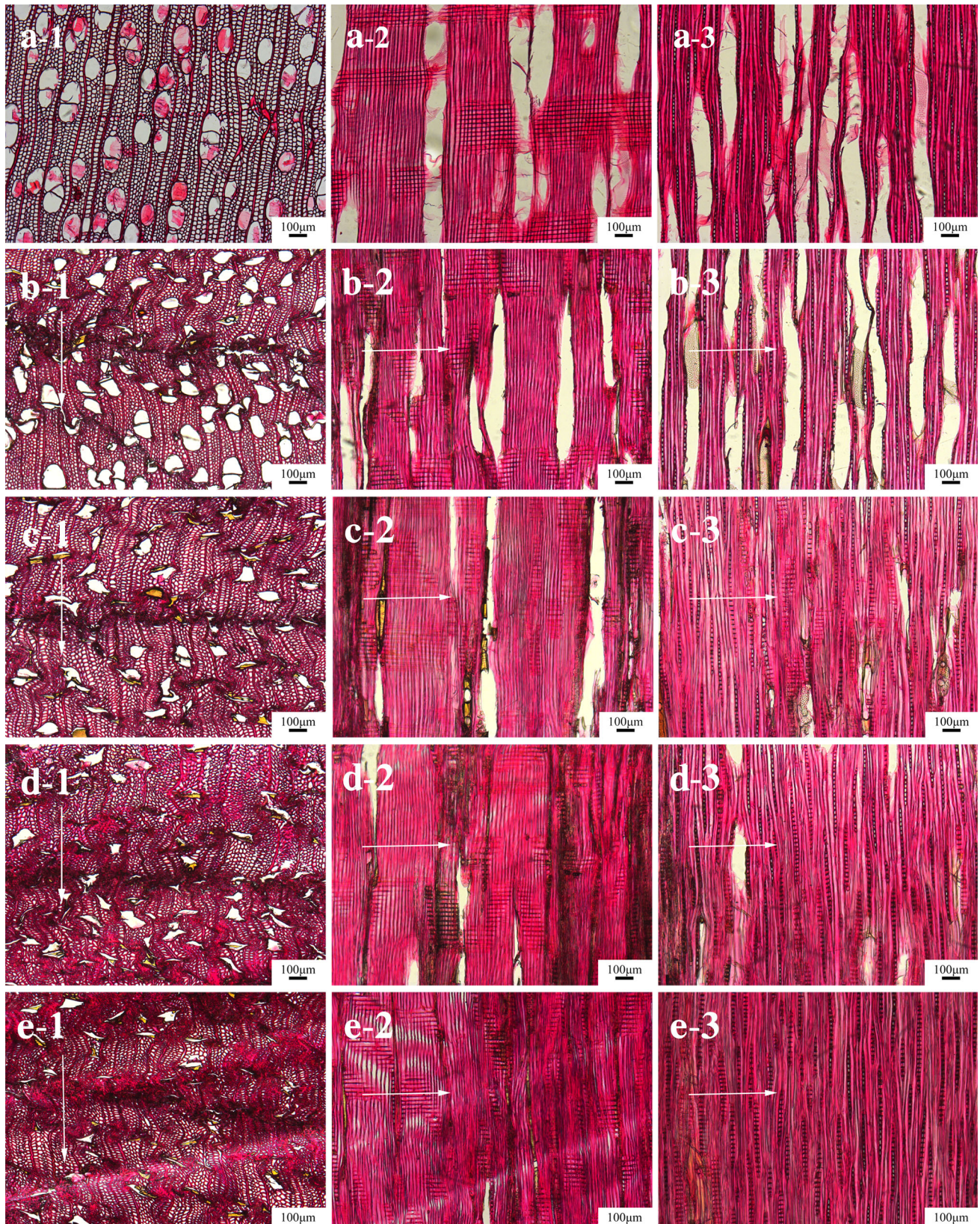


**Fig. 4** Photomicrographs on three sections (1 transverse section, 2 radial section, 3 tangential section) of untreated wood and compreg with four different densities: **a** untreated hybrid poplar; **b** 0.60 g/cm<sup>3</sup>;

**c** 0.80 g/cm<sup>3</sup>; **d** 1.00 g/cm<sup>3</sup>; **e** 1.20 g/cm<sup>3</sup>. The compression was in vertical direction as shown with arrows



**Fig. 5** SEM micrographs on longitudinal tangential section of **a** untreated hybrid poplar; **b** 1.20 g/cm<sup>3</sup> compreg. The inserted images (in white box) showing the pore were filled by adhesive

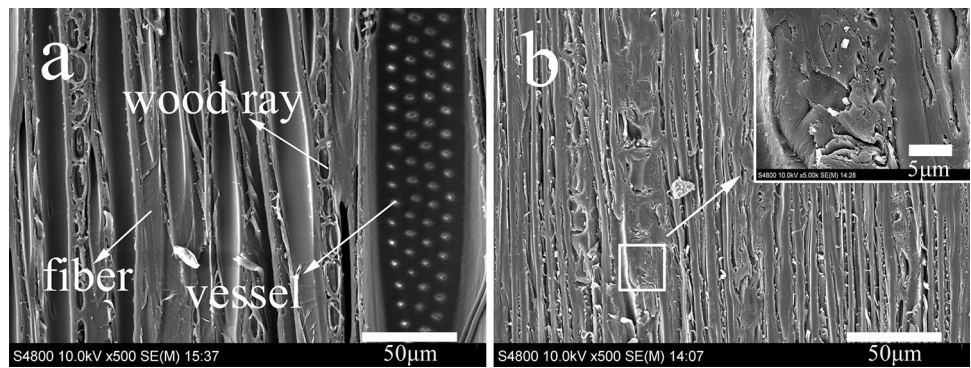


**Table 3** CT-analysis results for compregs with different densities

Density (g/cm <sup>3</sup> )	Theoretical porosity (%)	Total porosity (%)	MPS (µm)	SD of MPS (µm)
0.60	60.76	60.83	20.60	21.19
0.90	41.14	47.45	7.39	3.24
1.22	20.21	31.61	4.97	2.27

MPS mean pore size, SD of MPS standard deviation of mean pore size

total porosity, MPS, standard deviation (SD) of MPS was obtained using the µCT and shown in Table 3. The corresponding theoretical porosities were also calculated for comparison purpose. The total porosity represented the amount of the whole valid pores exhibited in the sample.

It can be observed that the total porosity was greater than that of theoretical porosity for all samples, respectively. The total porosity and MPS of compreg with the density of 0.60 g/cm<sup>3</sup> were larger than those of 0.90 and 1.22 g/cm<sup>3</sup>. This indicated that the 0.60 g/cm<sup>3</sup> sample had more valid pores compared to other two compregs, as shown in Table 3. The lower porosity confirmed that the cell cavity volume was already compressed and cells became more closely. The densification resulted in a significant decrease in the pore volumes. It is notable to mention that the SD value of MPS for 0.60 g/cm<sup>3</sup> compreg is extremely high. The pores between wood cells at this level of density maintain big sizes. Furthermore, the differences of the pore size between different wood cells are great. This resulted to the large standard deviation. Table 3 showed that the SD of MPS decreased with the increasing density of compregs.

The pore size distribution on the surface of the three compregs with different densities ranging from 0.88 to 25.46 µm was provided by the CTAn and shown in Fig. 6. The tendencies of pore distribution for the three samples were similar. The whole pore size distributions of the 0.90 and 1.22 g/cm<sup>3</sup> sample in Fig. 6 were concentrated more or less in relatively narrow peaks with the peak maximum at approximately 7.90 and 4.39 µm, respectively. These corresponded to the data for the

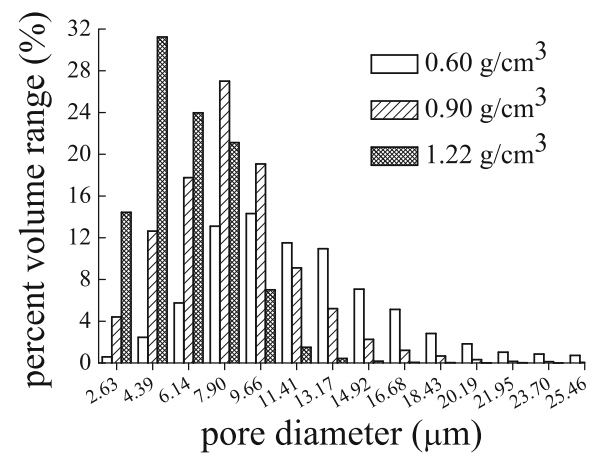


**Fig. 6** Results of pore size distribution by CT analyser (CTAn)

mean pore sizes (7.39 and 4.97 µm), as given in Table 3. Due to the densification, larger pores, such as wood ray cell lumina and vessel lumina, were compressed. Smaller pores, such as libriform fibers, were closer for compregs with higher densities. Vessels in compregs varied under compression. Their original structures were changed after compression and brought to the reduction in pore size, as shown in Fig. 6. Therefore, the pore area for the higher density samples (from 0.90 g/cm<sup>3</sup> to 1.22 g/cm<sup>3</sup>) was smaller than that of the 0.60 g/cm<sup>3</sup> samples, implying the loss in porosity as summarized in Table 3. This result was in agreement with the results reported in the previous publication [44].

## Conclusion

The results of the study revealed that the higher densities (ranging from 0.6 to 1.2 g/cm<sup>3</sup>) of compregs decreased their water absorption and improved the dimensional stability. The contact angles on the compreg surfaces were significantly greater than that of the untreated wood, indicating the low wettability character of the compreg. Both geometric mean model and acid–base model showed that total surface free energy decreased significantly with the increase of the compreg density. The smoothness of compreg surface was improved by densification. The surface characteristics were positively correlated with density. The microstructure analysis showed the higher density resulted in smaller porosity of the compreg, which led to the difficulty of the test liquid entering into the inner of sample. Moreover, Phenol–formaldehyde resin impregnation was successfully coupled with the compression process and consequently produced a dimensional stable wood-based product.

**Acknowledgments** The authors appreciate the financial support from the National Nonprofit Institute Research Grant of CAFINT (CAFINT2015C08).

## References

- State Forestry Administration of China (2014) Statistical year-book of forestry, Beijing
- Bal BC, Bektaş İ, Mengeloğlu F, Karakuş K, Demir HÖ (2015) Some technological properties of poplar plywood panels reinforced with glass fiber fabric. *Constr Build Mater* 101:952–957
- Baharoğlu M, Nemli G, Sarı B, Birtürk T, Bardak S (2013) Effects of anatomical and chemical properties of wood on the quality of particleboard. *Compos B* 52:282–285
- Xing C, Zhang S, Deng J, Riedl B, Cloutier A (2006) Medium-density fiberboard performance as affected by wood fiber acidity, bulk density, and size distribution. *Wood Sci Technol* 40:637–646
- Fang CH, Cloutier A, Blanchet P, Koubaa A (2012) Densification of wood veneers combined with oil-heat treatment. Part II: hygroscopicity and mechanical properties. *BioResources* 7:925–935
- Wei P, Wang BJ, Zhou D, Dai C, Wang Q, Huang S (2013) Mechanical properties of poplar laminated veneer lumber modified by carbon fiber reinforced polymer. *BioResources* 8:4883–4898
- Fang CH, Mariotti N, Cloutier A, Koubaa A, Blanchet P (2011) Densification of wood veneers by compression combined with heat and steam. *Eur J Wood Wood Prod* 70:155–163
- Fang CH, Cloutier A, Blanchet P, Koubaa A (2011) Densification of wood veneers combined with oil-heat treatment. Part I: Dimensional stability. *BioResources* 6:373–385
- Kutnar A (2007) Densification of wood. *Zbornik gozdarstva in lesarstva* 82:53–62
- Navi P, Heger F (2004) Combined densification and thermo-hydro-mechanical processing of wood. *MRS Bull* 29:332–336
- Inoue M, Norimoto M (2008) Fixation of compressive deformation in wood by pre-steaming. *J Trop For Sci* 20:273–281
- Sulaiman O, Salim N, Nordin NA, Hashim R, Ibrahim M, Sato M (2012) The potential of oil palm trunk biomass as an alternative source for compressed wood. *BioResources* 7:2688–2706
- Zhao Y, Wang Z, Iida I, Huang R, Lu J, Jiang J (2015) Studies on pre-treatment by compression for wood drying I: effects of compression ratio, compression direction and compression speed on the reduction of moisture content in wood. *J Wood Sci* 61:113–119
- Kamke FA, Sizemore Iii H (2008) Viscoelastic thermal compression of wood. US Patent Application No. 7.404.422
- Gabrielli CP, Kamke FA (2010) Phenol-formaldehyde impregnation of densified wood for improved dimensional stability. *Wood Sci Technol* 44:95–104
- Shams MI, Yano H (2010) Compressive deformation of phenol formaldehyde (PF) resin-impregnated wood related to the molecular weight of resin. *Wood Sci Technol* 45:73–81
- Deka M, Saikia CN (2000) Chemical modification of wood with thermosetting resin: effect on dimensional stability and strength property. *Bioresour Technol* 73:179–181
- Shams MI, Yano H (2004) Compressive deformation of wood impregnated with low molecular weight phenol formaldehyde (PF) resin II: effects of processing parameters. *J Wood Sci* 50:343–350
- Jennings JD, Zink-Sharp A, Frazier CE, Kamke FA (2006) Properties of compression-densified wood, Part II: surface energy. *J Adhes Sci Technol* 20:335–344
- Kutnar A, Kamke FA, Petrič M, Sernek M (2008) The influence of viscoelastic thermal compression on the chemistry and surface energetics of wood. *Colloids Surf Physicochem Eng Aspects* 329:82–86
- Chinese National Standard GB/T 17657 (2013) Test methods of evaluating the properties of wood-based panels and surface decorated wood-based panels. Standard Administration of China, Beijing
- Chinese National Standard GB/T 30364 (2013) Bamboo scrimber flooring. Standard Administration of China, Beijing
- Moura LFD, Hernández RE (2005) Evaluation of varnish coating performance for two surfacing methods on sugar maple wood. *Wood Fiber Sci* 37:355–366
- Moura LFD, Hernández RE (2006) Effects of abrasive mineral, grit size and feed speed on the quality of sanded surfaces of sugar maple wood. *Wood Sci Technol* 40:517–530
- Ayrlimis N, Winandy JE (2009) Effects of post heat-treatment on surface characteristics and adhesive bonding performance of medium density fiberboard. *Mater Manuf Processes* 24:594–599
- Owens DK, Wendt RC (1969) Estimation of the surface free energy of polymers. *J Appl Polym Sci* 13:1741–1747
- Oss CJV (1995) Hydrophobicity of biosurfaces-origin, quantitative determination and interaction energies. *Colloids Surf B* 5:91–110
- Oss CJV (1993) Acid-base interfacial interactions in aqueous media. *Colloids Surf A* 78:1–49
- Wu S (1971) Calculation of interfacial tension in polymer systems. *J Polym Sci Part C Polym Symp* 34:19–30
- Hacke UG, Sperry JS, Pockman WT, Davis SD, McCulloh KA (2001) Trends in wood density and structure are linked to prevention of xylem implosion by negative pressure. *Oecologia* 126:457–461
- Zhu RX, Yu WJ (2010) Effect of density on physical and mechanical properties of reconstituted small-sized bamboo fibrous sheet composite. *Adv Mater Res* 150:634–639
- Khalil HPSA, Bhat AH, Jawaid M, Amouzgar P, Ridzuan R, Said MR (2009) Agro-wastes: mechanical and physical properties of resin impregnated oil palm trunk core lumber. *Polym Compos* 31:638–644
- Yu YL, Huang XA, Yu WJ (2014) High performance of bamboo-based fiber composites from long bamboo fiber bundles and phenolic resins. *J Appl Polym Sci* 131:1–8

34. Diouf PN, Stevanovic T, Cloutier A, Fang CH, Blanchet P, Koubaa A, Mariotti N (2011) Effects of thermo-hygro-mechanical densification on the surface characteristics of trembling aspen and hybrid poplar wood veneers. *Appl Surf Sci* 257:3558–3564
35. Gindl M, Reiterer A, Sinn G, Stanzl-Tschegg SE (2004) Effects of surface ageing on wettability, surface chemistry, and adhesion of wood. *Holz Roh Werkst* 62:273–280
36. Šernek M, Kamke FA, Glasser WG (2005) Comparative analysis of inactivated wood surfaces. *Holzforschung* 58:22–31
37. Gérardin P, Petrič M, Petrissans M, Lambert J, Ehrhardt JJ (2007) Evolution of wood surface free energy after heat treatment. *Polym Degrad Stab* 92:653–657
38. Faust TD, Rice JT (1986) Effects of veneer surface roughness on gluebond quality in southern pine plywood. *For Prod J* 36:57–62
39. Kutnar A, Kamke FA (2010) Compression of wood under saturated steam, superheated steam, and transient conditions at 150°C, 160°C, and 170°C. *Wood Sci Technol* 46:73–88
40. Leclercq A, Riboux A, Jourez B (2001) Anatomical characteristics of tension wood and opposite wood in young inclined stems of poplar (*Populus euramericana* cv ‘Ghoy’). *Iawa J* 22:133–157
41. Kutnar A, Kamke FA, Šernek M (2008) Density profile and morphology of viscoelastic thermal compressed wood. *Wood Sci Technol* 43:57–68
42. Wan H, Kim MG (2006) Impregnation of southern pine wood and strands with low molecular weight phenol-formaldehyde resins for stabilization of oriented strandboard. *Wood Fiber Sci* 38:314–324
43. McBain J, Hopkins D (1925) On adhesives and adhesive action. *J Phys Chem* 29:188–204
44. Standfest G, Kutnar A, Plank B, Petutschnigg A, Kamke FA, Dunky M (2013) Microstructure of viscoelastic thermal compressed (VTC) wood using computed microtomography. *Wood Sci Technol* 47:121–139